THE ROYAL SOCIETY

How far can a juxtacrine signal travel?

Markus R. Owen[1], **Jonathan A. Sherratt**[2] **and Simon R. Myers**[3]

[1]*Department of Mathematics, University of Utah, Salt Lake City, UT 84112, USA* (*owen@math.utah.edu*)
[2]*Department of Mathematics, Heriot-Watt University, Edinburgh EH14 4AS, UK* (*jas@ma.hw.ac.uk*)
[3]*Academic Department of Dermatology, The Royal London Hospital, 2 Newark Street, London E1 2AT, UK*

Juxtacrine signalling is the process of cell communication in which ligand and receptors are both anchored in the cell membrane. We develop three mathematical models for this process, involving different mathematical representations of the dynamics of membrane-bound ligand and free and bound receptors, within an epithelial sheet. We consider the dynamics of this system following a localized disturbance, such as would be provided by a source of ligand or by the generation of a free edge via wounding. We study the ability of the juxtacrine mechanism to transmit a signal away from this disturbance, and show analytically that the spatial half-life of the signal can in fact be arbitrarily large. This result is quite general, since we use a generic reaction kinetic scheme; the key assumption is that ligand and receptor production are both upregulated by binding. Moreover, the result applies to all three of our model formulations. We conclude by discussing applications of the result to the particular case of the transforming growth factor alpha binding to epidermal growth factor receptor in epidermal wound healing.

Keywords: epidermis; juxtacrine; signal range; TGFα

1. INTRODUCTION

The term 'juxtacrine signalling' was coined by Massagué (1990) for a method of cellular communication in which signalling molecules anchored in the cell membrane bind to and activate receptors on the surface of immediately neighbouring cells. This is in contrast to the traditionally recognized activities of cell-signalling molecules, namely autocrine, paracrine and endocrine, meaning respectively that the molecules act only on the cell that secreted them, on nearby cells via extracellular diffusion and on all cells within a tissue. There are two main types of juxtacrine signalling molecule: (i) those that only exist in membrane-bound forms, such as the *Drosophila* proteins Boss and Delta, which bind to the receptors Sevenless and Notch (Lewis 1996); (ii) those that are membrane-bound precursors which undergo cleavage to give soluble paracrine ligands. In the latter case the relative rates of cleavage and decay of the membrane-bound form determine the relative importance of paracrine and juxtacrine signalling modes. Examples of this include epidermal growth factor (EGF), transforming growth factors α (TGFα) and β (TGFβ), and tumour necrosis factor. A more detailed review can be found in Massagué & Pandiella (1993).

Mathematical modelling of juxtacrine signalling was first considered by Collier *et al* (1996), focusing on the morphogenetic role of Delta–Notch signalling during *Drosophila* development. However, their model cannot be extended directly to most growth-factor juxtacrine signalling, because of assumptions made on protein and receptor release rates. Recently, Monk (1998) has adapted these previous models to study TGFβ juxtacrine signalling, with particular application to *Xenopus* mesoderm induction. His work indicates that for this system, there is an upper limit on the range over which the nearest neighbour signals can travel. This raises the important question of whether such a limited range is an intrinsic property of juxtacrine signalling. In this paper we study the rate at which signals decay in space, and show that the spatial half-life can be arbitrarily large.

We investigate the behaviour of signals propagated from a localized disturbance via juxtacrine signalling, using generic representations of growth factor production and binding. We will consider three different mathematical representations of the local averaging process implied by the juxtacrine mechanism; the key properties of our results apply to all three models, indicating that they are a function of the underlying biology rather than any mathematical details. The potential for long-range juxtacrine signalling is particularly important in the case of TGFα signalling away from the edge of epidermal wounds, and we illustrate our results with numerical simulations for parameters corresponding to this particular signalling system. In § 2, we introduce our three models, which are based on the same generic assumptions about the kinetics of ligand binding and the resulting feedback in ligand and receptor production—the differences between the models arise from different representations of juxtacrine communication. In § 3, we predict analytically the types of spatial signals that result when a stable homogeneous steady state is perturbed by a disturbance at a fixed location. We discuss the implications of the work in § 4.

2. MATHEMATICAL MODELLING OF JUXTACRINE SIGNALLING

We consider a two-dimensional sheet of cells, representing an epithelial sheet, with a linear disturbance of

Received 30 September 1998 *Accepted* 20 October 1998

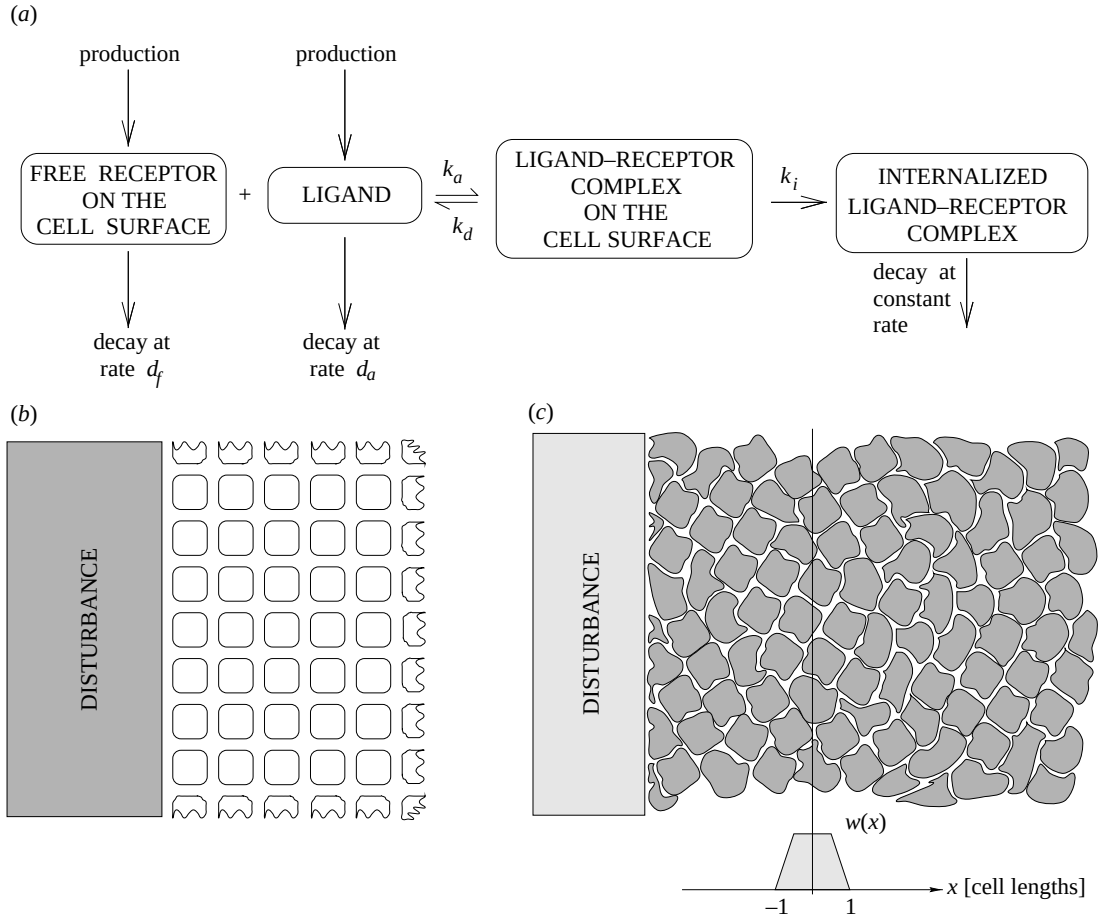

Figure 1. (*a*) The kinetic scheme used in our model for the binding of ligand to receptors, similar to that of Waters *et al*. (1990) for EGF–EGF-R interactions. (*b*) Schematic illustration of the model representation of the epithelium as a two-dimensional sheet of cells, indicating a linear disturbance such as would arise due to wounding. (*c*) When the cells are considered to be randomly distributed with varying shapes, the model variables can be considered as averages given by some spatial weighting kernel.

the normal growth factor and receptor equilibrium. Such a disturbance arises naturally in a variety of contexts, for example the localized secretion of ligand in development control and the generation of a free edge by epithelial wounding. We consider the behaviour as a function of perpendicular distance from the disturbance, ξ say, measured in units of epidermal cell lengths. Thus the variables are the cell surface density of ligand, free receptor and bound receptor, denoted by $a(\xi,t)$, $f(\xi,t)$, and $b(\xi,t)$, respectively. We will consider three alternative models, which differ in their representation of juxtacrine interactions between cells. In each case the basis of the model is a generic representation of ligand–receptor binding, as illustrated in figure 1*a*. This simple kinetic scheme is established as a good approximation for a number of growth factor–receptor interactions, with particularly detailed analysis for the binding of EGF to EGF-R (Waters *et al*. 1990; Starbuck & Lauffenburger 1992).

(a) *Model 1* (*discrete explicit*)

This involves a discrete representation of the cell sheet, with identical square cells making up a regular array; ξ takes integer values corresponding to the number of rows away from the disturbance, which is taken to be at row zero (figure 1*b*). This is similar to the modelling approach used by Collier *et al*. (1996) and Monk (1998). For our kinetic scheme, it gives the equations:

$$\partial a/\partial t = -k_a a\langle f\rangle + k_d\langle b\rangle - d_a a + P_a(b), \tag{1a}$$

$$\partial f/\partial t = -k_a\langle a\rangle f + k_d b - d_f f + P_f(b), \tag{1b}$$

$$\partial b/\partial t = k_a\langle a\rangle f - k_d b - k_i b, \tag{1c}$$

where P_a and P_f are feedback functions, whose form is discussed below. The notation $\langle\cdot\rangle$ indicates an average over neighbouring cells, defined by

$$\langle u(\xi,t)\rangle \equiv \frac{u(\xi-1,t)+2u(\xi,t)+u(\xi+1,t)}{4}. \tag{2}$$

This represents the total number of molecules available on the surface of the cells neighbouring a cell in row ξ. The term $2u(\xi,t)$ stems from our assumption that cells in the same row behave identically. We describe this model as 'explicit' because it includes non-local averages of the numbers of ligands, free receptors, and bound receptors which are explicitly active in the juxtacrine signalling process.

(b) *Model 2* (*continuous explicit*)

This model takes ξ as a real variable, with a continuum approximation made over a sheet of randomly distributed cells (figure 1*c*). Thus $a(\xi,t)$ denotes the ligand density on the surface of cells at distance ξ cell lengths from the disturbance. The model equations are the same as in equation (1) above, but with $\langle\cdot\rangle$ defined by

$$\langle u(\xi,t)\rangle = \int_{-\infty}^{\infty} \omega(s)u(s+\xi,t)\mathrm{d}s. \tag{3}$$

Here ω is a kernel which gives each point a weight according to its distance from the cell location ξ. This type of integral representation of non-local spatial interactions is widely used in ecological modelling (Neubert *et al*. 1995).

(c) *Model 3* (*continuous implicit*)

This again involves a continuum approximation over the cell sheet, with ξ a real variable, but with a different representation of the juxtacrine interaction. In model 2, we assumed that ligand and receptor were distributed uniformly over the surface of a cell. However, in practice they may be expressed non-uniformly over the surface and can also move over the cell while remaining membrane bound; this latter phenomenon has been modelled mathematically by Gex-Fabry & Delisi (1984). In our final model, we consider an extreme case of this, in which all kinetic reactions and production terms act pointwise in space, but with production occurring as a function of the overall receptor number on a cell. This gives equations

$$\partial a/\partial t = -k_a af + k_d b - d_a a + P_a(\langle b\rangle), \tag{4a}$$

$$\partial f/\partial t = -k_a af + k_d b - d_f f + P_f(\langle b\rangle), \tag{4b}$$

$$\partial b/\partial t = k_a af - k_d b - k_i b, \tag{4c}$$

where $\langle\cdot\rangle$ is defined by equation (3). Here the interpretation of the variables is different from model 2, with $a(\xi,t)$ representing the density of ligand at the point ξ, rather than the average density on the surface of cells centred at ξ (and similarly for b and f).

We assume that the cell sheet is initially at a homogeneous equilibrium (a_e,f_e,b_e) (all non-zero); there is always at least one such equilibrium in model 1. Juxtacrine signals are then induced by a boundary condition which perturbs this homogeneous steady state:

$$(a(\xi),f(\xi),b(\xi)) = (a^*,f^*,b^*) \neq (a_e,f_e,b_e) \quad \text{for all } \xi \leqslant 0. \tag{5}$$

Our interest in spatial signal ranges stems from this disturbance, which does not allow the homogeneous steady state as a solution to model 1. Instead, solutions perturbed at the boundary evolve to a steady state which varies in space, gradually approaching the homogeneous steady-state level as the distance from the disturbance increases.

(d) *Specification of feedback functions*

Recall that P_a and P_f are the production rates of ligand and receptor respectively, which we assume to be increasing functions of the number of bound receptors on the cell surface, reflecting positive feedback. This makes our model fundamentally different from that of Collier *et al*. (1996), who assume down-regulation of ligand expression as a result of receptor binding on the cell surface; this is a special property of the Delta–Notch system they are considering. Numerical simulation of course requires specification of particular functional forms for P_a and P_f, and for the figures we have used Hill functions (details in figure legends). However, our analysis will be quite general. Since our calculations involve linearizing about the homogeneous steady state, the feedback functions enter only through their slopes at $b = b_e$, that is $\mathcal{A} = P_a'(b_e)$ and $\mathcal{F} = P_f'(b_e)$. Our approach in the remainder of the paper will be to treat the kinetic parameters as having fixed (but arbitrary) values, and to determine the behaviour as a function of the parameters $\mathcal{A}$ and $\mathcal{F}$.

In the special case of a spatially homogeneous epithelium, all three models reduce to the same system of three coupled ordinary differential equations. The range of possible feedback functions is constrained by the requirement that the homogeneous steady state (a_e,f_e,b_e) is stable as a solution of these equations—otherwise the concept of signal range is not relevant. Standard stability analysis shows that this requires $\mathcal{F}$ to lie below two lines $\mathcal{L}_1$ and $\mathcal{L}_2$ in the $\mathcal{A}$–$\mathcal{F}$ plane, defined mathematically in equations (A1) and (A2) in Appendix A. Detailed analysis (summarized in Appendix A) shows that $\mathcal{L}_1$ and $\mathcal{L}_2$ can intersect in four possible ways, depending on parameter values, giving the stability regions illustrated in figure 2.

3. ANALYSIS OF THE SIGNAL RANGE

Intuitively, one expects that the strength of the feedback in the ligand and receptor production terms would affect the range over which a signal is propagated away from a perturbation, and this is confirmed by numerical simulations of all three models (representative simulations of the continuous explicit model are illustrated in figure 3). In order to quantify this dependence, we will consider in this section the spatial half-life of steady-state solutions decaying towards the homogeneous equilibrium. This provides a convenient measure of signal range that can be calculated analytically.

(a) *Predicting spatial decay rates* (*explicit models*)

We wish to predict the rate at which steady-state solutions decay in space towards the homogeneous steady state—the solution is perturbed away from this homogeneous state by the localized disturbance. We consider models 1 and 2 together, and discuss model 3 separately below. At steady state, the model equations (1) give three equations in space only. We linearize these equations about the homogeneous steady state (a_e,f_e,b_e), and look for decaying solutions of the form $a(\xi) = \bar{a}\mathrm{e}^{\lambda\xi}$, etc, where $\bar{a}$ is constant.

Substituting these into the linearized equations leads to the following condition for non-trivial solutions

$$\begin{aligned}\mathcal{K}_m(\lambda)^2\{d_f k_d + k_a k_i a_e - k_a a_e\mathcal{F}\}k_a f_e + \mathcal{K}_m(\lambda)\{d_f k_a f_e\mathcal{A}\}\\ -\{d_f k_i + d_f k_d + k_a k_i a_e - \mathcal{F}\}(k_a f_e + d_a) = 0,\end{aligned} \tag{6}$$

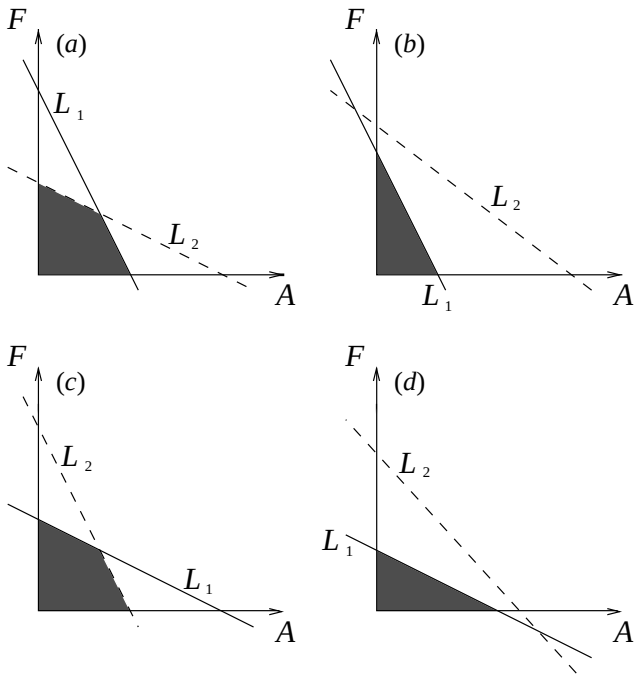

Figure 2. Schematic indicating the possible configurations of the line $\mathcal{L}_1$ (solid) and the line $\mathcal{L}_2$ (dashed). The region under both lines is such that the homogeneous steady state is temporally stable to homogeneous perturbations, and the solid line also coincides with a zero spatial decay rate. Parts (*a*) and (*b*) are all the possibilities for $d_a < d_f$, in which case line $\mathcal{L}_1$ has a more negative slope than line $\mathcal{L}_2$. Similarly, for $d_a > d_f$, the possibilities are cases (*c*) and (*d*). This means that whatever our kinetic parameters it is never the case that an instability of the homogeneous steady state can prevent solutions with zero decay rate.

where the subscript m denotes the model type: d for discrete, c for continuous, with $\mathcal{K}_d(\lambda) \equiv (\cosh(\lambda)+1)/2$ and $\mathcal{K}_c(\lambda) \equiv \int_{-\infty}^{\infty} \omega(s) e^{\lambda s} ds$. Intuitively, $\mathcal{K}_m$ represents the contribution of neighbouring cells to the signal propagation.

We denote the roots of equation (6) for $\mathcal{K}_m(\lambda)$ as $\mathcal{K}_+$ and $\mathcal{K}_-$; the set of permissible decay rates λ is given by the set of solutions of $\mathcal{K}_m(\lambda) = \{\mathcal{K}_+, \mathcal{K}_-\}$. Note that the $\mathcal{K}_m(\lambda)$ are even functions, so the decay rates will come in pairs of opposite sign, reflecting the spatial isotropy of the model. We expect the decay rate observed in practice in model solutions to be given by the pair of solutions with the smallest magnitude, since all linear modes will be present; intuitively, this is just saying that solutions will decay as slowly as they can. Figure 4 illustrates the accuracy of this analysis in comparison with numerical simulations of the full model equations.

It is exactly the relationship between $\mathcal{K}_d(\lambda)$ and $\mathcal{K}_c(\lambda)$ which determines the difference between the discrete and continuous explicit models in terms of the rate at which their steady-state solutions decay in space towards the homogeneous equilibrium. The analysis of $(\mathcal{A},\mathcal{F})$ space in terms of the solutions $\{\mathcal{K}_+, \mathcal{K}_-\}$ is identical, with the only differences in predicted decay rates arising from the different values of λ that $\mathcal{K}_c(\lambda)$ and $\mathcal{K}_d(\lambda)$ give as inverses of $\{\mathcal{K}_+, \mathcal{K}_-\}$. In fact, with the kernel $\omega(s) = (\delta(s+1) + 2\delta(s) + \delta(s-1))/4$, the continuous model reduces exactly to the discrete model.

(b) *Predicting spatial decay rates (implicit model)*

As for the explicit models, we linearize the equations for the time-independent system about the spatially homogeneous steady state, and substitute perturbations proportional to $\exp(\lambda\xi)$. Imposing the requirement of non-trivial solutions gives the condition

$$\mathcal{K}_c(\lambda) = \frac{k_a k_i (d_a a_e + d_f f_e) + d_a d_f (k_d + k_i)}{(k_a d_f f_e \mathcal{A} + k_a d_a a_e \mathcal{F})}. \tag{7}$$

Hence for a given parameter set we may solve for λ, and the values predicted by this analysis are in close agreement with decay rates calculated from numerical simulation of the full equations (see figure 4).

(c) *What is the maximum signal range?*

Large signal ranges correspond to the decay rate λ being small. In such cases $\mathcal{K}_d(\lambda)$ and $\mathcal{K}_c(\lambda)$ can be expanded as power series, enabling relatively simple approximations for λ to be derived. Applying this procedure gives the following expressions for the half-life of decay, $\mathcal{H}$ say $(= \ln 2/\lambda)$, for the three models:

model 1

$$\mathcal{H} = \left\{ \frac{k_a f_e (2(d_f k_d + k_a k_i a_e) + d_f \mathcal{A} - 2k_a a_e \mathcal{F}) \ln 2}{d_a d_f (k_d + k_i) + k_a k_i (d_a a_e + d_f f_e) - d_f k_a f_e \mathcal{A} - d_a k_a a_e \mathcal{F}} \right\}^{1/2}, \tag{8}$$

model 2

$$\mathcal{H} = \sqrt{2\Gamma} \left\{ \frac{k_a f_e (2(d_f k_d + k_a k_i a_e) + d_f \mathcal{A} - 2k_a a_e \mathcal{F}) \ln 2}{d_a d_f (k_d + k_i) + k_a k_i (d_a a_e + d_f f_e) - d_f k_a f_e \mathcal{A} - d_a k_a a_e \mathcal{F}} \right\}^{1/2}, \tag{9}$$

model 3

$$\mathcal{H} = \sqrt{2\Gamma} \left\{ \frac{(k_a d_f f_e \mathcal{A} + k_a d_a a_e \mathcal{F}) \ln 2}{d_a d_f (k_d + k_i) + k_a k_i (d_a a_e + d_f f_e) - k_a d_f f_e \mathcal{A} - k_a d_a a_e \mathcal{F}} \right\}^{1/2}. \tag{10}$$

where $\Gamma = \int_{-\infty}^{+\infty} \omega(s) s^2 ds$. The key feature of these formulae is that the denominator inside the square root is the same in all cases, and is precisely zero on $\mathcal{L}_1$; recall that the homogeneous equilibrium becomes unstable as parameters are varied across this line. Since $\mathcal{L}_1$ always forms part of the boundary of the stability domain (see figure 2), the signal half-life becomes arbitrarily large within the stability domain, for parameters sufficiently close to the line $\mathcal{L}_1$. Figure 4 illustrates the accuracy of these approximations, and shows how the half-life of decay increases dramatically as $\mathcal{A}$ approaches $\mathcal{L}_1$. There is an important caveat to this result, however. Since the line $\mathcal{L}_1$ corresponds to marginal stability of the homogeneous equilibrium, a long-range signal will require a long time-scale to be established. In reality, maximum signal range within a given finite time will correspond to parameters slightly away from the line $\mathcal{L}_1$, reflecting a compromise between signal range and evolution time.

Note that the signal range predicted by the discrete and continuous explicit models depend in the same way on kinetic parameters, with any difference due to the details of the spatial kernel $\omega(\cdot)$. This is as expected, since these models are based on identical biological assumptions. The formula for the implicit model is

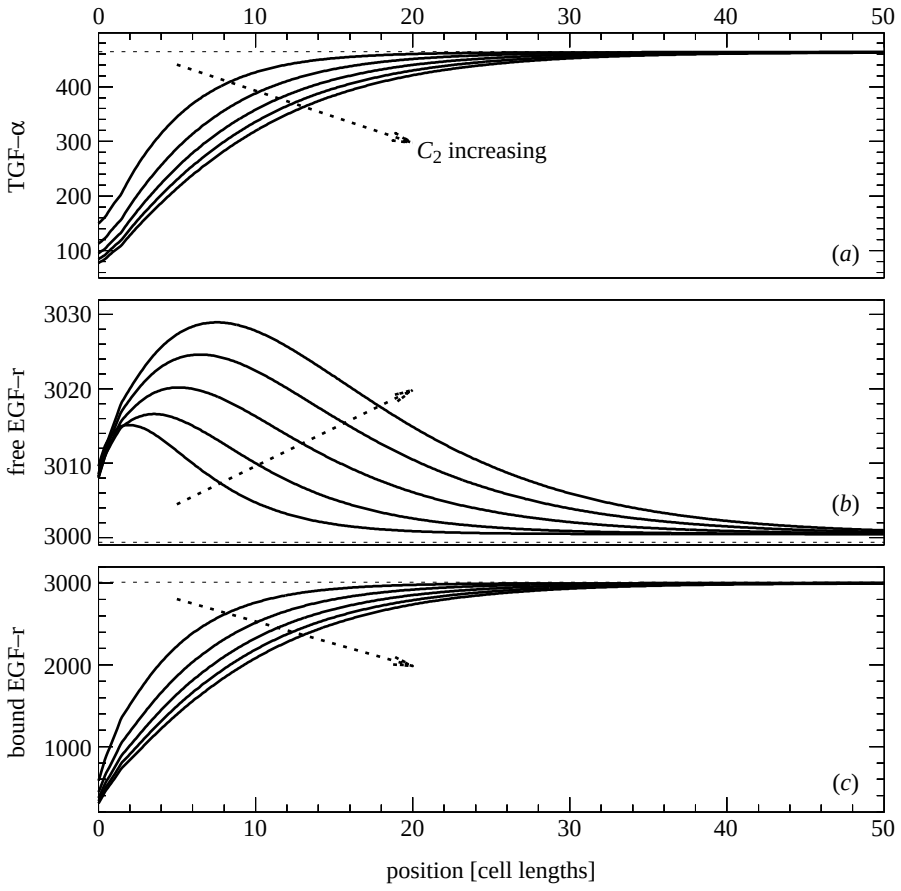

Figure 3. Numerically calculated solutions of the continuous explicit juxtacrine model (defined by equations (1) and (3)), specified with feedback functions $P_a(b) = C_1 b/(C_2 + b)$, $P_f(b) = C_3 + C_4 b/(C_5 + b)$. The kernel used was piecewise constant, with $\omega(\xi) = 0$ for $\xi \in (-\infty, -3/2)$, $\omega(\xi) = 1/4$ for $\xi \in [-3/2, -1/2)$, $\omega(\xi) = 1/2$ for $\xi \in [-1/2, 1/2]$, $\omega(\xi) = 1/4$ for $\xi \in (1/2, 3/2]$, and $\omega(\xi) = 0$ for $\xi \in (3/2, \infty)$. The solutions are shown after 166.7 h (10 000 min) of evolution with the wounded boundary condition (equation (5)), for C_2 increasing from 10 000 to 50 000 at intervals of 10 000. The distance of propagation of the wound-induced perturbation clearly increases as the parameter C_2, and hence the strength of feedback in TGFα production, increases. The other parameters are $k_a = 0.0003$ molecules^{-1} min^{-1}, $k_d = 0.12\,\text{min}^{-1}$, $k_i = 0.019\,\text{min}^{-1}$, $d_a = 0.006\,\text{min}^{-1}$, $d_f = 0.03\,\text{min}^{-1}$, $f_e = 3000$, $b_e = 3000$, $r_0 = 3000$, $r_m = 25\,500$. Although in our analysis we treat the domain as semi-infinite, we can only simulate a finite range of cells, N, so we impose the right-hand boundary condition $a(\xi) = a(N), (\xi) = f(N)$, $b(\xi) = b(N)$ for all $\xi > N$. This is not significant provided N is sufficiently large.

different, reflecting the assumption of non-uniform receptor expression over the surface of the cell, but the key property of arbitrarily long signal half-life holds for all three cases.

The expressions (8–10) are based on the assumption of a simple monotone decay away from a localized disturbance. In fact, for the explicit models, such a disturbance can generate solutions other than monotonic decay. Mathematically, this arises because there are solutions of equation (6) which imply complex values of λ. This allows for two additional signal types, namely oscillatory decay, and propagating patterns. A detailed mathematical study of these cases for the discrete version of the explicit model can be found in (Owen & Sherratt 1998). In contrast the implicit model (model 3) always implies simple decaying solutions.

4. DISCUSSION

The central conclusion from this work is that for any juxtacrine signalling system with our highly generic ligand–receptor kinetics, solutions which decay from some disturbance to a homogeneous steady state can have an arbitrarily large signal half-life, independent of the details of the spatial coupling. A system in which the range of a juxtacrine signal is particularly important is the TGFα–EGF-R interaction in epidermal wound healing. In adult mammals, such wounds heal by a combination of cell crawling at the wound edge, and enhanced proliferation further back (for review, see Martin 1996). Although this combined mechanism of healing was established many years ago (e.g. Winter 1972), the underlying molecular details remain unclear. TGFα, which acts via binding to EGF-R in a mainly juxtacrine manner, has traditionally been considered to be an important element in the epidermal wound healing process in humans. Normal human keratinocytes produce TGFα both *in vivo* and *in vitro* (Coffey *et al.* 1987), and TGFα upregulates both migration and proliferation of keratinocytes in culture (Barrandon & Green 1987). Moreover, addition of exogenous TGFα accelerates epithelial wound healing. The kinetic binding scheme illustrated in figure 1 is well established for this particular ligand–receptor interaction, and there is extensive previous modelling work on which kinetic parameters can

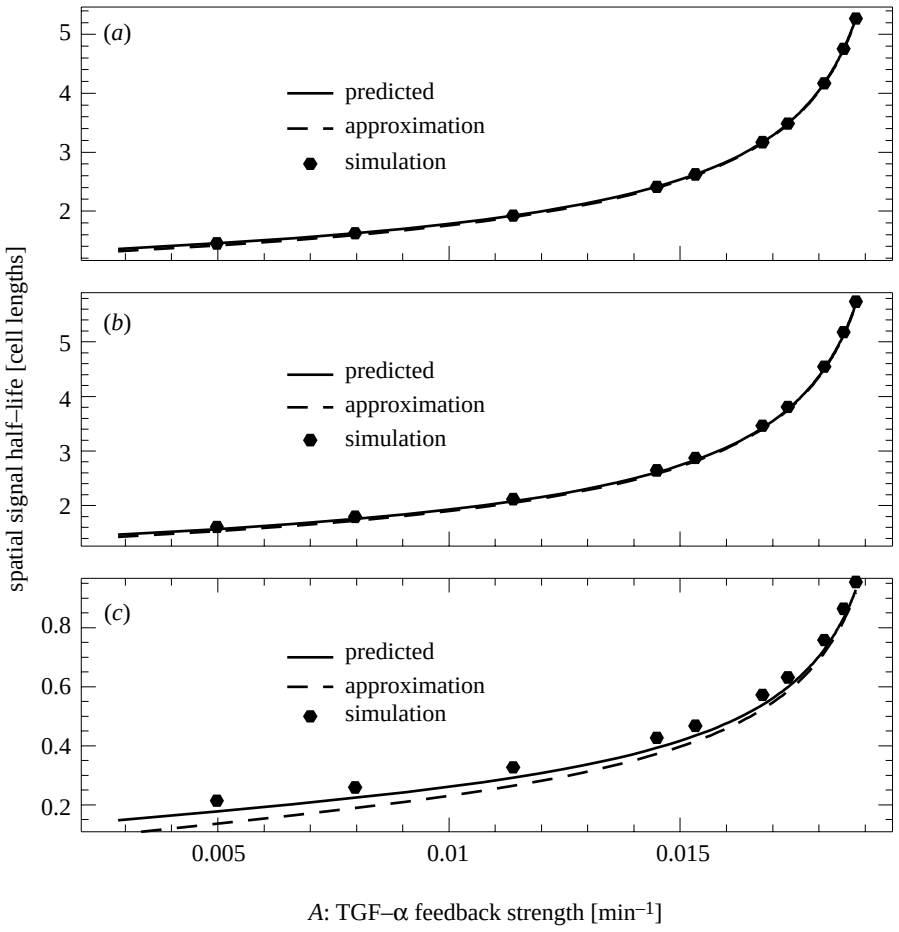

Figure 4. Spatial half-lives ($= \ln 2/\lambda$) as a function of TGFα feedback strength, $\mathcal{A}$, for three models of juxtacrine signalling. Note the close agreement between analytical predictions, approximations (8–10), and half-lives calculated from numerical simulations. As expected, the signal range increases dramatically as $\mathcal{A}$ approaches 0.01994, which corresponds to the line of marginal stability, $\mathcal{L}_1$. The values from simulations were calculated by simulating for 10 000 min from an initially homogeneous steady state with the wounded boundary condition. The basic model details and parameters are as in figure 3, except that C_2 was varied from 2000 up to 50 000 to achieve the illustrated variation in $\mathcal{A}$. Model 2 (continuous explicit) used the same kernel as described in the legend to figure 3, and model 2 (continuous implicit) used the piecewise linear kernel given by $\omega(\xi) = 0$ for $\xi \in (-\infty, -1)$, $\omega(\xi) = 4(1+\xi)/3$ for $\xi \in [-1, -1/2)$, $\omega(\xi) = 2/3$ for $\xi \in [-1.2, 1/2]$, $\omega(\xi) = 4(1-\xi)/3$ for $\xi \in (1/2, 1]$, and $\omega(\xi) = 0$ for $\xi \in (1,\infty)$. (*a*) Discrete explicit; (*b*) continuous explicit; (*c*) continuous implicit.

be based; our numerical simulations illustrated in figures 2–4 have all used parameters determined in this way (details in figure legends).

The question of the range of TGFα activity in epidermal repair is raised by recent work of Werner and co-workers (Werner *et al.* 1992, 1994), showing a large induction of (KGF) by dermal fibroblasts as an early response to wounding. KGF is a member of the fibroblast growth factor family, and stimulates the proliferation of keratinocytes (see Tsuboi *et al.* (1993) and Pierce *et al.* (1994) for quantitative data) by binding to KGF-R; this receptor is upregulated in the epidermis following wounding (Werner *et al.* 1992; Marchese *et al.* 1995). Since it is produced in the relatively acellular papillary dermis, KGF has the potential to exhibit long-range activity via extracellular diffusion, consistent with the observed increase in cell division over many cell diameters from the wound edge. Our results show that TGFα acting in a juxtacrine manner may be as important in mitotic upregulation as KGF, even at sites quite distant from the wound edge. The key determinant of this role is the strength of the feedback in TGFα and EGF-R expression, corresponding to $\mathcal{A}$ and $\mathcal{F}$ in the model. Experi-mental measurement of these parameters *in vitro* is quite feasible, using an approach similar to that developed by Kudlow *et al.* (1986) for measuring EGF-R upregulation by EGF binding. This data, combined with our modelling results, would enable a detailed comparison of the relative contributions of TGFα and KGF to mitotic upregulation as a function of distance from the edge of an epidermal wound.

A key feature of the work in this paper is the detailed comparison of discrete and continuous models for the same phenomena. Spatially discrete models are an increasingly important tool in cell biology, enabling detailed modelling that reflects the cellularity of the tissue concerned. The relatively simple situation of signalling in an epithelium with stationary cells enables our discrete model to be studied analytically. More generally, discrete models tend to be a computational tool, but have nevertheless been used very effectively to study cell rearrangements in development (Weliky *et al.* 1991) and

the aggregation of cellular slime moulds (Savill & Hogeweg 1997; Van Oss *et al*. 1996; Dallon & Othmer 1997). Within the context of wound healing, the natural extension of our work is to develop an enlarged model framework including cell movement and proliferation, and receptor diffusion. For such an extended model, the continuous formulation is the simplest to use, enabling direct inclusion of existing continuum models for these processes (Sherratt & Murray 1990; Gex-Fabry & Delisi 1984). The very close agreement of the continuum model with the discrete representation in the basic context that we consider provides strong evidence that it is a realistic representation of the juxtacrine signalling process.

M.R.O. was supported in part by an earmarked studentship from the Engineering and Physical Sciences Research Council. We thank John Dallon for helpful discussions.

APPENDIX A

In this Appendix we briefly summarize the arguments showing that the only possible regions of the $\mathcal{A}$–$\mathcal{F}$ parameter plane in which the homogeneous steady state (a_e,f_e,b_e) is stable are those illustrated in figure 2. Standard linear analysis shows that stability is determined by the roots of a cubic polynomial. Applying the Routh–Hurwitz conditions gives two inequalities which must be satisfied for all the roots to have negative real part, and hence for the homogeneous steady state to be stable. These inequalities determine two lines which bound the region of stability, $\mathcal{L}_1$ and $\mathcal{L}_2$, given by

$$\mathcal{L}_1\colon \mathcal{F} = k_i + \frac{d_f(k_d+k_i)}{k_a a_e} + \frac{k_i d_f f_e}{d_a a_e} - \frac{d_f f_e}{d_a a_e}\mathcal{A}, \tag{A1}$$

$$\mathcal{L}_2\colon \mathcal{F} = k_i + d_a + \frac{d_f f_e}{a_e} + \frac{d_a d_f + (k_d+k_i)(d_a+d_f)}{k_a a_e} + \frac{d_a^2(d_f+k_d+k_i) + (k_a a_e + k_a f_e + k_d + k_i + 1)k_a k_i f_e + (d_f f_e + d_a a_e)k_a}{(d_f + k_a a_e + k_a f_e + k_d + k_i)k_a a_e} - \frac{f_e(d_a + k_a a_e + k_a f_e + k_d + k_i)}{a_e(d_f + k_a a_e + k_a f_e + k_d + k_i)}\mathcal{A}. \tag{A2}$$

These lines both have negative slopes and are positive when $\mathcal{A}=0$. Their relative gradients depend on the relationship between d_a and d_f: for $d_a<d_f$, independent of the other kinetic parameters, the line $\mathcal{L}_1$ has a more negative gradient than line $\mathcal{L}_2$; for $d_a>d_f$, the opposite is true. Note that the region under *both* lines is stable, with the homogeneous steady state unstable otherwise. Calculation of the values of $\mathcal{A}$ and $\mathcal{F}$ at which $\mathcal{L}_1$ and $\mathcal{L}_2$ intersect shows that $\mathcal{A}>0$ at intersection if $d_a>d_f$ and $\mathcal{F}>0$ at intersection if $d_f>d_a$. This restricts the possible configurations to those illustrated in figure 2.

REFERENCES

Collier, J. R., Monk, N. A. M., Maini, P. K. & Lewis, J. H. 1996 Pattern formation by lateral inhibition with feedback: a mathematical model of delta–notch intercellular signalling. *J. Theor. Biol*. **183**, 429–446.

Dallon, J. C. & Othmer, H. G. 1997 A discrete cell model with adaptive signalling for aggregation of dictyostelium discoideum. *Phil. Trans. R. Soc. Lond*. B **352**, 391–417.

Gex-Fabry, M. & Delisi, C. 1984 Receptor mediated endocytosis: a model and its implications for experimental analysis. *Am. J. Physiol*. **247**, R768–R779.

Kudlow, J. E., Cheung, C. M. & Bjorge, J. D. 1986 Epidermal growth factor stimulates the synthesis of its own receptor in a human breast cancer cell line. *J. Biol. Chem*. **261**, 4134–4138.

Lewis, J. 1996 Neurogenic genes and vertebrate neurogenesis. *Curr. Opin. Neurobiol*. **6**, 3–10.

Martin, P. 1996 Mechanisms of wound healing in the embryo and fetus. *Curr. Topics Devl. Biol*. **32**, 175–203.

Massagué, J. 1990 Transforming growth factor-α: a model for membrane-anchored growth factors. *J. Biol. Chem*. **265**, 21 393–21 396.

Massagué, J. & Pandiella, A. 1993 Membrane-anchored growth factors. *A. Rev. Biochem*. **62**, 515–541.

Monk, N. A. M. 1998 Restricted-range gradients and travelling fronts in a model of juxtacrine cell relay. *Bull. Math. Biol*. **60**, 901–918.

Neubert, M. G., Kot, M. & Lewis, M. A. 1995 Disperal and pattern formation in a discrete-time predatot-prey model. *Theor. Popul. Biol*. **48**, 7–43.

Owen, M. R. & Sherratt, J. A. 1998 Mathematical modelling of juxtacrine cell signalling *Math. Biosci*. **152**, 125–150.

Savill, N. J. & Hogeweg, P. 1997 Modelling morphogenesis: from single cells to crawling slugs. *J. Theor. Biol*. **184**, 229–235.

Sherratt, J. A. & Murray, J. D. 1990 Models of epidermal wound healing. *Proc. R. Soc. Lond*. B **241**, 29–36.

Starbuck, C. & Lauffenburger, D. A. 1992 Mathematical model for the effects of epidermal growth factor receptor trafficking dynamics on fibroblast proliferation response. *Biotechnol. Prog*. **8**, 132–143.

Van Oss, C., Panfilov, A. V., Hogeweg, P., Siegert, F. & Weijer, C. J. 1996 Spatial pattern formation during aggregation of the slime mould dictyostelium discoideum. *J. Theor. Biol*. **181**, 203–213.

Waters, C. M., Oberg, K. C., Carpenter, G. & Overholser, K. A. 1990 Rate constants for binding, dissociation, and internalization of EGF: effect of receptor occupancy and ligand concentration. *Biochemistry* **29**, 3563–3569.

Weliky, M., Minsuk, S., Keller, R. & Oster, G. 1991 Notochord development in xenopus laevis: simulation of cell behaviour underlying tissue convergence and extension. *Development* **113**, 1231–1244.

As this paper exceeds the maximum length normally permitted, the authors have agreed to contribute to production costs.